EUROfusion

EUROFUSION WPJET1–PR(14)08

C. Reux et al.

Runaway Electron Beam Generation and Mitigation During Disruptions at JET-ILW

Preprint of Paper to be submitted for publication in
Nuclear Fusion

This work has been carried out within the framework of the EUROfusion Consortium and has received funding from the Euratom research and training programme 2014-2018 under grant agreement No 633053. The views and opinions expressed herein do not necessarily reflect those of the European Commission.

Runaway electron beam generation and mitigation during disruptions at JET-ILW

C. Reux[1], V. Plyusnin[2], B. Alper[3], D. Alves[2], B. Bazylev[4], E. Belonohy[5], A. Boboc[3], S. Brezinsek[6], J. Decker[1], P. Drewelow[7], S. Devaux[3], P. de Vries[8], A. Fil[1], S. Gerasimov[3], L. Giacomelli[3], S. Jachmich[9], E.M. Khilkevitch[10], V. Kiptily[3], R. Koslowski[6], U. Kruezi[3], M. Lehnen[8], I. Lupelli[3], A. Manzanares[11], A. Martin De Aguilera[11], G. Matthews[3], J. Mlynář[12], E. Nardon[1], E. Nilsson[1], V. Riccardo[3], F. Saint-Laurent[1], A.E. Shevelev[10], C. Sozzi[13], JET contributors‡

EUROfusion Consortium, JET, Culham Science Centre, Abingdon, OX14 3DB, UK
[1]CEA, IRFM, F-13108 Saint-Paul-lez-Durance, France
[2]Instituto de Plasmas e Fuso Nuclear, IST, Universidade de Lisboa, Lisboa, Portugal
[3]CCFE, Culham Science Centre, Abingdon OX14 3DB, UK
[4]IHM, Karlsruhe Institute of Technology, Campus Nord,76021 Karlsruhe, Germany
[5]EFDA-CSU, Culham Science Centre, Abingdon OX14 3DB, UK
[6]Forschungszentrum Jülich GmbH, Institut fr Energie-und Klimaforschung-Plasmaphysik, 52425 Jlich, Germany
[7]Max-Planck-Institut for Plasma Physics; Wendelsteinstr. 1 17489 Greifswald, Germany
[8]ITER Organization, Route de Vinon sur Verdon, 13115 St Paul Lez Durance, France
[9]Laboratoire de Physique des Plasmas-Association EURATOM-Belgian State Institute ERM/KMS, B-1000 Brussels, Belgium
[10]Ioffe Physical-Technical Institute of the Russian Academy of Sciences, Polytechnicheskaya 26, St Petersburg, 194021, Russia
[11]Association Euratom-CIEMAT, Moncloa Avd. Complutense 22 28040 Madrid 3, Spain
[12]Institute of Plasma Physics AS CR, Za Slovankou 3, 18200 Prague 8, CZ
[13]Istituto di Fisica del Plasma CNR-EURATOM, via Cozzi 53, 20125 Milano, Italy

E-mail: `cedric.reux@cea.fr`

Abstract. Disruptions are a major operational concern for next generation tokamaks, including ITER. They may generate excessive heat loads on plasma facing components, large electromagnetic forces in the machine structures and several MA of multi-MeV runaway electrons. A more complete understanding of the runaway generation processes and methods to suppress them is necessary to ensure safe and reliable operation of future tokamaks. Runaway electrons were studied at JET-ILW showing that their generation dependencies (accelerating electric field, avalanche critical field, toroidal field, MHD fluctuations) are in agreement with current theories.

‡ See the Appendix of F. Romanelli et al., Proceedings of the 25th IAEA Fusion Energy Conference 2014, Saint Petersburg, Russia

In addition, vertical stability plays a key role in long runaway beam formation. Energies up to 20 MeV are observed. Mitigation of an incoming runaway electron beam triggered by massive argon injection was found to be feasible provided that the injection takes place early enough in the disruption process. On the contrary, suppressing an already accelerated runaway electron beam in the MA range was found to be difficult even with injections of more than 2 kPa.m^3 high-Z gases such as krypton or xenon. This may be due to the presence of a cold background plasma weakly coupled to the runaway electron beam which prevents neutrals from penetrating in the electron beam core. Following unsuccessful mitigation attempts, runaway electron impacts on beryllium plasma-facing components were observed, showing localized melting with toroidal asymmetries.

1. Introduction

Disruptions are a major threat for future tokamaks including ITER. They have 3 kinds of consequences. Electromagnetic forces are induced by eddy currents or halo currents and can damage internal components or induce stress in the vacuum vessel. Heat loads on plasma facing components may exceed the material limits and damage the first wall or divertor surface. Relativistic runaway electrons (RE) up to 20 MeV can be accelerated during the current quench with currents up to more than half the initial plasma current. These electrons form a beam which can be sustained for up to 100 milliseconds to several seconds on present tokamaks. The beam impact on plasma facing components leads to localized in-depth heat loads spread over a few millimeter thickness and carries the risk of damaging more fragile structures behind the first wall tiles (coolant pipes, support structures). Consequently, prevention of runaway electron generation or suppression of runaway electron beams once they are created are essential on ITER. This aims at ensuring safe and reliable plasma operations and avoiding long downtime periods needed by repairs. Runaway electrons have been studied on many machines in the world since early tokamaks ([1]) but also on recent larger machines such as JET [2, 3, 4, 5], JT-60U [6, 7], Tore Supra [8, 9], TEXTOR [10, 11], DIII-D [12, 13, 14], FTU [15], TFTR [16]. Experiments have focused on documenting their generation conditions as a function of operational or physics parameters. In particular, it has been demonstrated that the generation rate of runaway electrons increases more than linearly with the machine size [17, 18]. Common operational dependencies include the pre-disruption density, the toroidal field B_t and the initial plasma current I_p. Physics dependencies include the electron density during the disruption and the accelerating electric field. These are captured by the current models for runaway generation: the Dreicer mechanism and the avalanche mechanism. Other physics dependencies related to the runaway losses are the magnetic fluctuations [19] or some plasma instabilities [20, 21]. A number of methods to suppress runaways have been studied worldwide: resonant magnetic perturbations [11] or massive material injection [22, 23, 24, 25, 26]. Due to the difficulties with generating reliable and reproducible runaway electrons beams, only a few attempts have been made to try to suppress a fully-blown runaway electron beam [8, 14], with only limited success.

The present article describes recent runaway electrons studies on the European tokamak JET with its ITER-Like Wall configuration. The paper is organized as follows. Section 1 describes the background for runaway electrons at JET and the experimental setup used in recent studies. Section 2 addresses the runaway electron operational domain at JET-ILW and focuses on operational and physics dependencies of runaway electrons. Section 3 is focused on runaway mitigation attempts, either before the runaway beam generation (i.e. runaway electron *prevention*) or after the generation of the runaway beam (i.e. runaway electron *suppression*). It also gives some insight on the runaway beam physics in its environment during disruptions mitigated with massive gas injection. Section 4 reports on observations of runaway electrons impacts on plasma facing components and mechanisms leading to the final loss of the runaway current.

2. Experimental background and setup

2.1. Runaway electron background at JET

Runaway electrons used to be observed on a regular basis during disruptions at JET with its carbon wall configuration. Runaway beams up to 1.2 MA have been observed in high current disruptions in the past [27] with the JET carbon wall (JET-C). In more recent dedicated experiments, runaway beams up to 50 ms have also been obtained by argon injection using standard gas valves [3] or massive injections of heavy gases by the first Disruption Mitigation Valve (DMV1). It was observed that the runaway electron plateau regime differed depended on the way it was created. Runaway beams triggered by slow gas injection tended to have steady runaway current with almost no photoneutron emission until the final current drop. On the contrary, runaway electron beams created by massive gas injection of argon showed a slow decrease of the plasma current and a steady neutron/HXR emission throughout the whole plateau duration, with still a final drop of the current in the end. This behavior was attributed to the interaction between the runaway beam and the gas from massive injection. Since the installation of the ITER-Like Wall at JET (JET-ILW) with its tungsten divertor and beryllium first wall limiters, runaway generation during spontaneous disruptions dropped significantly. In more than 7000 pulses from the first JET-ILW campaigns, only two pulses showed low-energy runaways (so-called *slideaways*) during a very low-density current ramp-up following a gas introduction system failure. A couple of other pulses showed trace of low energy electrons in low-density discharges. The absence of runaway electrons in JET-ILW disruptions was attributed to slower current quenches (CQ). This is due to the fact that plasma radiation is much lower in JET-ILW disruptions due to the absence of carbon as a radiating impurity. The optimum radiation temperature for beryllium (now the main impurity at JET-ILW) is higher than the carbon one; this leads to a hotter plasma during the current quench and hence a lower accelerating electric field leading to less runaway electrons. This feature is also believed to be responsible for the inability to generate runaway beams with slow argon injections as it was the case in

carbon wall as mentioned above.

2.2. Experimental setup and methods

Runaway electrons in recent JET campaigns have been studied mainly using the two JET Disruption Mitigation Valves (DMV1 and DMV2). Both are eddy current valves developed at FZ Jülich. DMV1 is located on the top of a 4 meter narrow tube on an upper port of JET octant 1 as shown on figure 1. Its volume is 650 ml and it can inject up to 1000 Pa.m^3 deuterium when filled at maximum pressure (3.3 MPa) [28]. The injection volume is not completely emptied during injections due to the dynamics of the opening piston. Heavier gases like argon have a lower throughput than lighter ones and take more time to reach the plasma due to a lower sound speed. The second disruption mitigation valve (DMV2) is located on the midplane of octant 3 at the end of a shorter (2.4 m) and wider (75 mm diameter) tube. Its plenum volume is 975 ml [29] and the valve opening is larger (15 mm versus 5 mm for DMV1) thus giving shorter response time and larger throughput than DMV1. Maximum filling pressure is 5.0 MPa leading to a maximum injection of 5 kPa.m^3 deuterium. Its use is however restricted to lower values in normal operations in order to avoid a too large heat influx on the divertor cryopumps. This is due to the heat conducted to the cryo panels by the injection gas filling the vacuum vessel. Cryo pumping has to be switched off to use the valve at maximum pressure. Details on the gas flow dynamics and throughputs can be found in the reference articles mentioned for each valve. Both DMVs are able to inject deuterium, hydrogen, helium, neon, argon, krypton, xenon or mixtures of D_2/H_2 and heavier gases. In addition DMV2 is compatible with tritium operations. Most of the runaway electron disruptions analyzed in the present article have been triggered by massive injections of heavy gases (argon). On the contrary to methods involving low density plasmas either current during ramp-up or involving seed suprathermal populations (ECCD or LHCD), argon MGI tends to produce fairly reliable runaway beams.

The implantation of the main diagnostics used in this article's study is described on figure 1. A fast far infrared interferometer is located in octant 7 with 3 vertical chords for density measurements during the disruptions up to the MHz acquisition frequency. Chord setup is given on figure 1(b). Two bolometer arrays are located in octant 3 and octant 6 with vertical and horizontal lines of sight respectively and capture the total power radiated by the plasma. High resolution magnetic probes located in octant 3 are used to measure MHD fluctuations. Soft X-ray arrays are used to track the low-energy runaway emission and are located in octant 4. A fast visible camera is located in octant 8 and provides a wide-angle view of the vacuum vessel including the DMV1 injection port. A fast infrared camera located in the same area provides surface temperature maps of the runaway impacts on plasma facing components. Hard X-ray (HXR) cameras and spectrometers located in octant 1 and 8 on the top of the torus measure the HXR and neutrons energy spectrum used to determine the runaway energy. 3 pairs of fission chambers (octants 1-2, octants 6-7, octants 7-8) give the total neutron yield during the

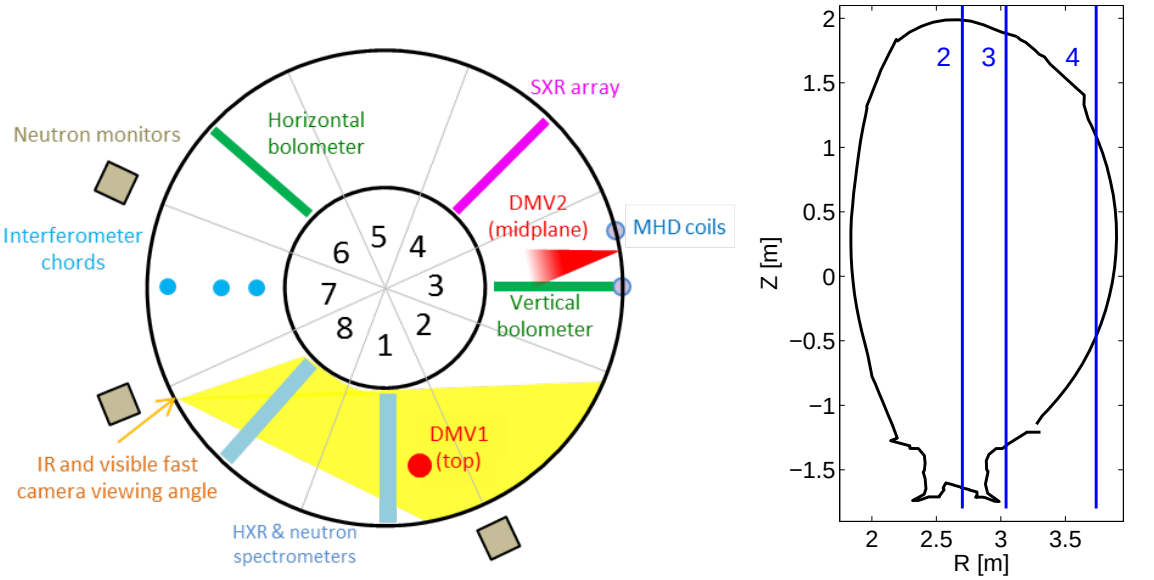

Figure 1. Implantation of diagnostics and Disruption Mitigation Valves on JET (a) top view (b) Interferometer chords

disruption. Most of the post-disruption neutrons are photoneutrons in the cases studied in the present article.

3. Runaway characterization - existence domain

3.1. Operational existence domain

Runaway electrons are very rare in spontaneous disruptions in JET-ILW due to slower current quenches related to the intrinsic impurity content of the plasma. The runaway existence domain can however be studied using massive injections of mixtures of deuterium and argon from the DMVs. The injected impurities dominate over the intrinsic beryllium content of the post-disruption plasma. This yields a larger range of fast current quench as well as a better control of the runaway electron generation conditions. DMVs are used in daily operations as routine protection systems with a 10% argon+90% deuterium mixture known not to produce any runaway electrons. Due to its high sound speed, deuterium mixes quickly into the plasma and helps increasing the electron density enough to curb runaway acceleration. In addition, its low radiation efficiency [30] does not produce fast current quenches generating large accelerating electric fields. Conversely, pure argon injection are known to produce large amounts of runaways in JET-C era experiments due to the poor mixing efficiency of argon and the very fast current quenches it produces.

The runaway existence domain was thus mapped using different D_2+Ar mixtures in various pressures, different toroidal fields, plasma pre-disruption densities and shapes. The summary of this existence domain is mapped on figure 2. The domain boundary for divertor configurations is given for JET-C and JET-ILW as red and green eye-guiding

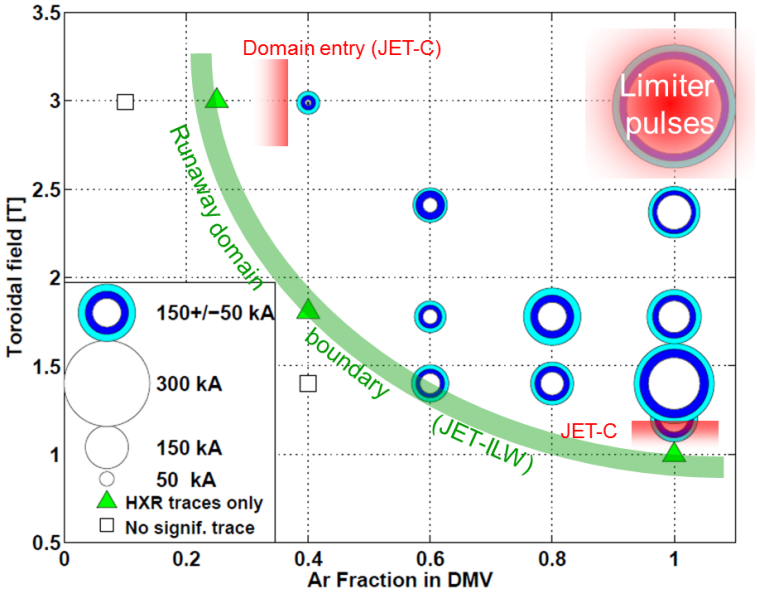

Figure 2. Runaway electron existence domain map as a function of toroidal field and argon fraction in the disruption mitigation valve. The domain entry points/boundaries is given for JET-C and JET-ILW. Circle size indicates the maximum runaway current reached during the disruption

lines. One can see that the entry points into the existence domain are similar between JET-C and JET-ILW in divertor configurations. As discussed earlier, triggering the runaway beam using massive gas injection significantly negates the effect of the wall impurity during the first part of the disruption. One can also notice that limiter low-elongation disruptions lie within the same region as the divertor configurations. However they produce larger amounts of runaways for the same toroidal field and argon fractions. This will be addressed in the next section.

It is to be noted that the maximum runaway current for points inside the domain (100% argon) is larger in 5 out of 6 cases in JET-ILW than in JET-C. This is attributed to lower densities at the end of the current quench [31]. Fuel retention is indeed much lower at JET-ILW than JET-C; lower outgassing after the disruption radiation flash may be responsible for lower electron densities at the end of the current quench (when the injected impurity may be less dominant on the plasma content) thus leading to higher amounts of runaway electrons.

3.2. Physics dependencies

3.2.1. Methodology. Runaway generation and loss are related to a number of mechanisms each depending on physics quantities such as electron density, electric field, etc. In order to be able to extrapolate the existence domain at JET-ILW to other devices, the dominating mechanisms and their dependencies should be identified. Runaways are generated through two main processes. Primary generation is linked to

the Dreicer mechanism [32, 33]. It is related to the electric field threshold $E_D = \frac{n_e e^3 \ln\Lambda}{4\pi\epsilon_0^2 m_e T_e}$, where n_e is the electron density, T_e the electron temperature and $ln\Lambda$ is the coulombian logarithm. A relativistic correction was proposed in cases where the speed needed for an electron to run away was close to the speed of light [34]. The critical field $E_c = \frac{n_e e^3 \ln\Lambda}{4\pi\epsilon_0^2 m_e c^2}$ represents the ultimate threshold below which no electron can run away. Note that cases where the accelerating electric field E_a lies within $E_c < E_a < E_D$ may lie within conditions where the growth rate of the runaway population is well below the timescale of the disruption. The second runaway generation process is the knock-on avalanche mechanism where an already accelerated runaway electron transfers enough energy to a thermal electron during a collision to make it run away [17]. This mechanism depends on the same critical field E_c as mentioned above. One of the main dependencies for runaway electron generation is thus the ratio between the accelerating electric field and the critical electric field, the latter being proportional to the electron density. Other indirect but known dependencies are the toroidal field B_t [7, 27] and magnetic fluctuations [19]. For the cases presented in this article, the accelerating electric field is calculated using a 0D coupled circuits calculation which takes into account plasma, vacuum vessel and poloidal field coils. The following system is solved, assuming constant mutual inductances and neglecting the effect of the JET iron core.

$$\begin{cases} E = \frac{1}{2\pi R}\left[L_p \frac{dI_p}{dt} + \sum M_{coils,plasma}\frac{dI_{coils}}{dt} + \sum M_{struct,plasma}\frac{dI_{structures}}{dt}\right] \\ \sum_{i,j,i\neq j} M_{i,j}\frac{dI_j}{dt} + R_i I_i + L\frac{dI_i}{dt} = 0 \end{cases} \quad (1)$$

Taking into account only the plasma current derivative to compute the accelerating electric field would lead to an overestimation of 50% to 100%, underlining the importance of a full calculation. The density needed in the critical field calculation is taken from interferometry measurements. Unfortunately, large density gradients and fluctuations at the thermal quench lead to a loss of signal early in the current quench. Consequently, the last valid density measurements before the thermal quench are used for the critical field calculation. In order to keep measurements consistent between discharges where the density signal is lost at different times, the data point used for the calculation is chosen at the same time distance to the thermal quench for all pulses (namely 1.4 ms).

3.2.2. Runaway existence domain. Results are summarized on figure 3 showing a map of the runaway existence domain as a function of the electric fields ratio and the toroidal magnetic field. One can see that for divertor pulses, two clear regions can be distinguished: low accelerating field ratios and low toroidal field do not give rise to substantial amounts of runaway electrons, whereas high toroidal fields and high accelerating electric field ratios yield high runaway electron currents. This is in agreement with the known dependencies of runaway generation and confirms that JET-ILW is not different from JET-C on this aspect. However, the limiter pulses do not follow the domain separation as shown on figure 3. For equivalent E_a/E_c ratios, they yield much higher runaway currents than divertor pulses. This proves that the plasma shape matters during runaway acceleration. It also confirms the general trend that

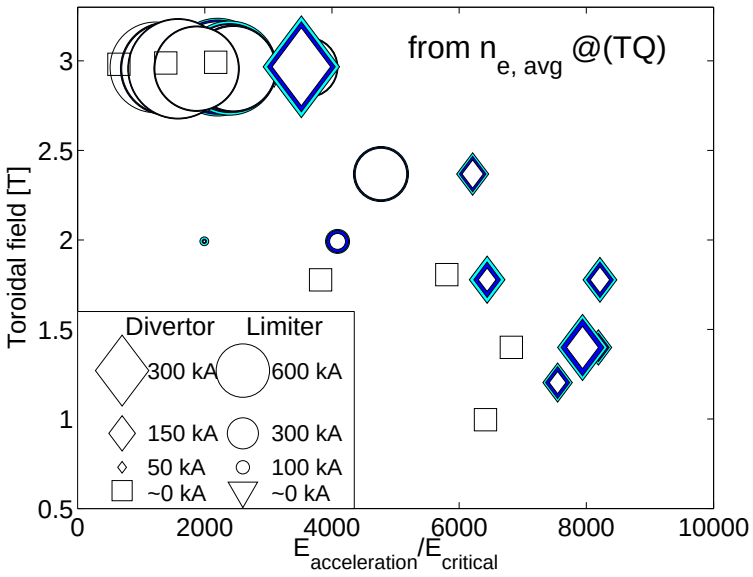

Figure 3. Runaway electron existence domain map as a function of toroidal field and ratio of accelerating electric field over the critical electric field. Marker size indicates the magnitude of the runaway current.

limiter or low-elongation machines produce large amounts of runaway electrons easily [35] whereas elongated machines can produce substantial amounts of runaways only by triggering disruptions in low elongation plasmas [14].

The influence of magnetic turbulence was also investigated using high-resolution MHD coils on the low field side of the vacuum vessel (see figure 1). The mean value of normalized magnetic fluctuations $\delta B/B$ between 1.5 ms after the thermal quench and the time when the plasma current reaches 2/3 of its pre-disruption value are used for this study. A map of the runaway currents as a function of the electric fields ratio and the magnetic fluctuations is shown on figure 4. As with the previous runaway domain map, one can see that two domains can be distinguished : high magnetic fluctuations can only yield large runaway amounts if the electric field ratio is large enough. Limiter cases tend to have lower magnetic fluctuations than divertor ones which may be part of the reason why runaway currents are much higher in limiter configurations than divertor ones. However, divertor pulses with similar ($\delta B/B$, E_a/E_c) as most of the limiter cases do exist and did not produce any significant amounts of runaways. Consequently magnetic fluctuations (although being lower in limiter cases) cannot alone explain the observed difference. Three particular points in the magnetic fluctuations map have to be noted as they have much larger fluctuations than any other. They correspond to runaway beams triggered by the second disruption mitigation valve DMV2 which has a larger throughput than DMV1 (which is used to trigger all the other disruptions in this dataset). Magnetic fluctuations are much more pronounced for those three disruptions. Two of them did not show any significant runaway currents despite being full argon injections. Those two pulses represent the only cases at JET where a massive injection

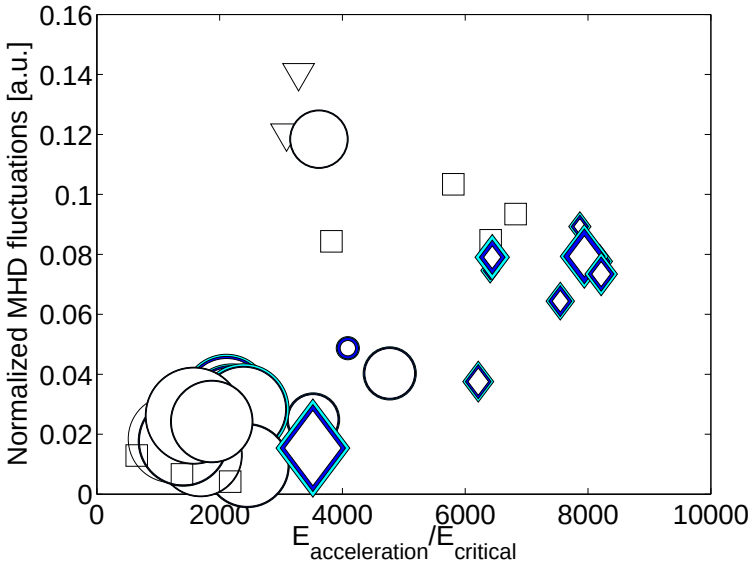

Figure 4. Runaway electron existence domain map as a function of normalized magnetic fluctuations and ratio of accelerating electric field over critical electric field. Marker size indicates the magnitude of the runaway current.

of pure argon (330 and 1020 Pa.m^3 respectively) did not generate a significant amount of runaways. Nevertheless, the fact that the third DMV2 (879 Pa.m^3) pulse in this dataset produced a 660 kA runaway beam shows that magnetic fluctuations are not the only reason why runaway generation is suppressed in some cases.

3.3. Runaway electron energies

Runaway electron energies are calculated from HXR and neutron spectra measurements. The HXR energy distribution is then deconvoluted using the DeGaSum code [36] in order to obtain the runaway energy spectrum. Two spectra examples are given on figure 5 for a 150 kA runaway beam from a divertor plasma disruption and a 580 kA semi-plateau beam from a limiter disruption. Up to 20 MeV runaways are produced, in the usual range for large tokamaks. The maximum energy saturates quickly around 150 kA of runaways. Only runaway beams with currents lower than $\approx$ 100 kA see a decrease in their maximum energy.

4. Runaway electron beam mitigation

4.1. Runaway beam scenario characterization

In order to perform runaway beam mitigation experiments, a reliable runaway beam scenario has been developped at JET-ILW. The disruption is triggered by a massive injection of pure argon using the first Disruption Mitigation Valve (DMV1) on a low elongation outer limiter plasma ($\kappa \approx 1.32$). The amount of argon injected ranges from

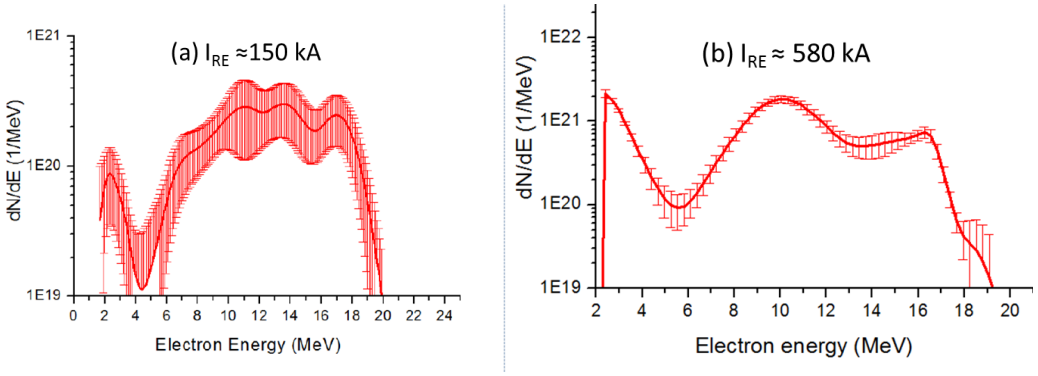

Figure 5. Examples of two deconvoluted runaway spectra. (a) Short 150 kA runaway beam from a divertor configuration (b) 580 kA semi-plateau from a limiter configuration

60 Pa.m^3 to 410 Pa.m^3. This leads to 0.7-1.0 MA runaway beams lasting between 30 and 100 ms. An example of such a beam is given on figure 6. One has to note that the runaway current steadily decreases during the plateau phase. This is attributed to the interaction between the runaway beam and the large amount of neutral gas which has been injected by DMV1 to trigger the disruption. This interaction can be seen by the approximately constant HXR activity during the whole beam phase. Direct interaction with the wall might be an explanation, but runaway beams created using slow standard argon injection in JET-C era did not exhibit such a large HXR activity throughout the runaway beam phase. This tends to show that the massive gas puff itself is responsible for the HXR emission. Runaway beams at JET tend to slowly drift inwards and upwards. Reconstruction of the confined plasma (including the runaway beam) boundary was made using the position of the current centroid and assuming constant elongation after the disruption. Snapshots of the boundary shape are given on figure 6. A detailed analysis of the runaway impacts on the wall will be presented in section 5.

An important feature of this runaway beam scenario is the background plasma generated behind it. The runaway beam evolves within a cold plasma with a significant free electron density. It is clearly visible on the density signals from the far infrared interferometer (figure 6 (e) and (f)). One has to note that the density measurements during the plateau phase are only relative. Since the fringe reference is lost just after the thermal quench, only relative evolutions can be inferred from the signal. The reconstruction from the end of the pulse cannot be made either since the signal is generally lost again at the runaway beam impact on the wall. The relative density signal can however be used as a lower bound for the actual absolute density value. Electron densities up to 3×10^{20} m^{-2} can be observed on chords 2 and 3 (figure 6 (e)), with a steady increase. The density cannot be only due to runaway electrons themselves; a rough estimate of the number of runaways based on the beam size as given by the contact points calculation 6(b) is given by $n_{RE} = I_{RE} * (2\pi * R)/ecV_{RE} \approx 1.2 \times 10^{16}\mathrm{m}^{-3}$, which

is far less than the free electron density measurements show on figure 6. The interaction between the runaway beam and the cold background plasma is also visible on the fast camera pictures, with an increasing visible emission correlated with the expected beam position (see figure 6(h)). Moreover, this background plasma is not limited to the confined region where the runaway beam is expected to be. The interferometer chord n4 which is far away from the supposed confined region also measures densities up to $5 \times 10^{19} m^{-3}$ (see figure 6(f)). This is an indication that this background plasma fills a major part of the vacuum vessel. The maximum density measured by this edge chord seems to be relatively independent of the amount injected by DMV1 (see figure 7). This tends to show that the background plasma features are probably determined by an ionization balance rather by the amount of gas injected, as discussed below.

This runaway electron beam heals the poloidal field structure during the plateau phase and provides confinement for the cold background plasma. As a consequence, this plasma does not need to carry a large toroidal current to be confined. Background plasma and RE beam are however weakly coupled by collisions between relativistic electrons and neutrals or ions coming from the pre-disruptive plasma. These collisions are actually responsible for the creation of the background plasma itself. This density build-up was observed on Tore Supra during RE beams [8] and is confirmed to a larger extent at JET.

Assuming an uniform spreading of the DMV1 injection gas into the vacuum vessel and connected volumes (307 m^3) the amount of argon available for ionisation through collisions with REs can be estimated to 1.24×10^{20} m^{-3} Argon thus dominates the post-disruption plasma inventory by at least a factor 5 compared to the pre-disruption deuterium content (mean value 2.5×10^{19} m^{-3}). Outgassing from the wall is neglected in this simple calculation, since it was found to be much lower for JET-ILW than for JET-C [37]. A simple model can be build to understand the mechanism underlying the density build-up during the runaway beam. Part of the collisions between runaways and background neutrals will lead to ionizations. In addition, the runaway current steadily decreases, giving rise to a toroidal electric field of about 2-2.5 V/m in the case shown on figure 6. Loss of energy per unit length by the runaway beam (the so called stopping power) can be calculated using the ESTAR code [38] using excitation energies recommended by [39]. This stopping power is shown on figure 8 together with the accelerating electric force during the plateau phase. For low energies ($\leq 1MeV$), slowing down is dominated by electron-atoms collisions. For higher energies, bremsstrahlung losses dominate. Losses by collisions which mainly depend on the relative speed between electron and atom become independent on the energy. As pointed out by Bakhtiari et al [40], the stopping power reaches a minimum for RE energy around 1 MeV. As a consequence, provided that the accelerating electric force power is larger than the minimum stopping power, the following situations may arise:

- If the RE energy is lower than E_{K1} (see figure 8), it will be slowed down to the thermal distribution;

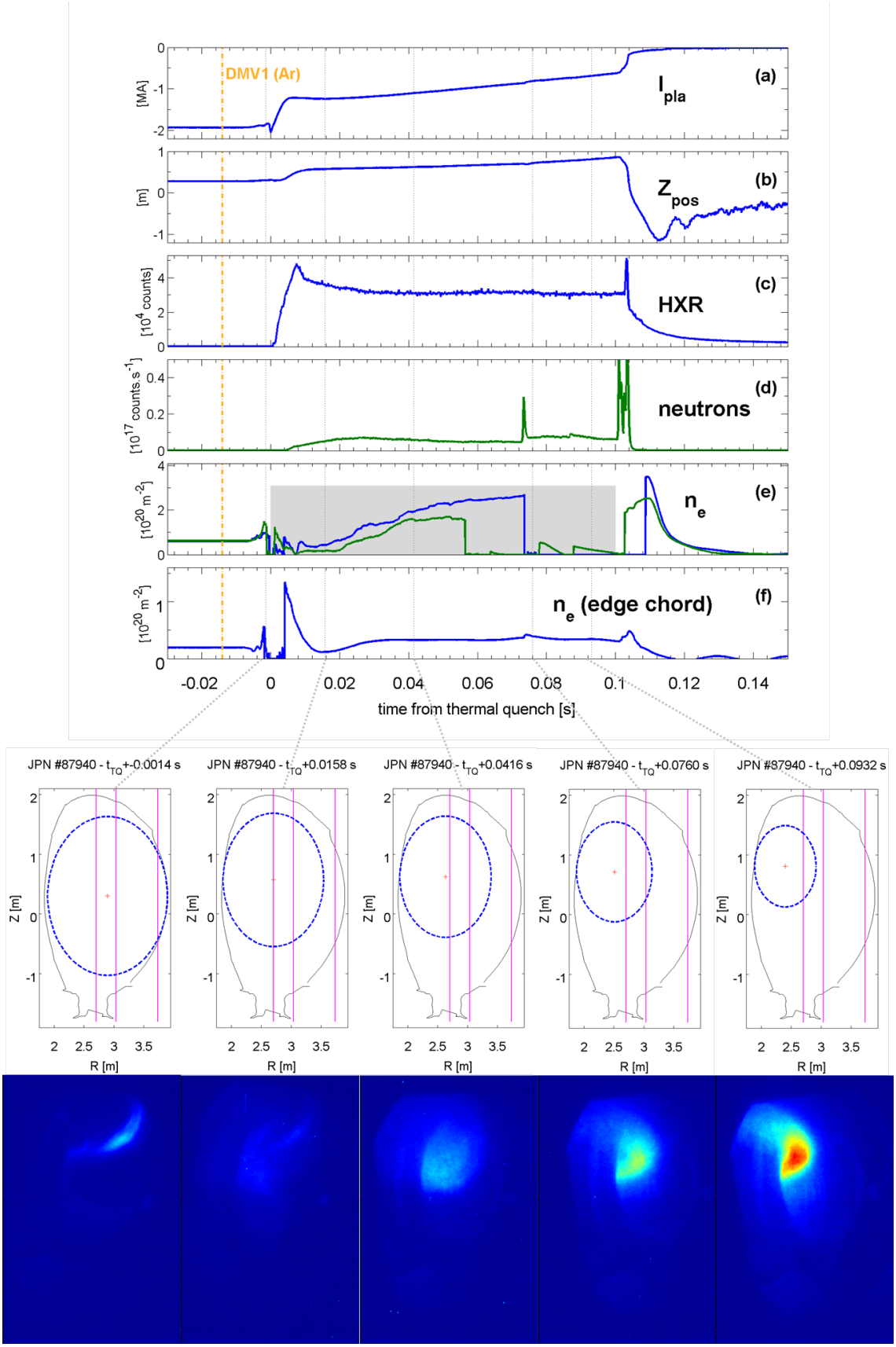

Figure 6. Runaway beam scenario example (JPN87940).

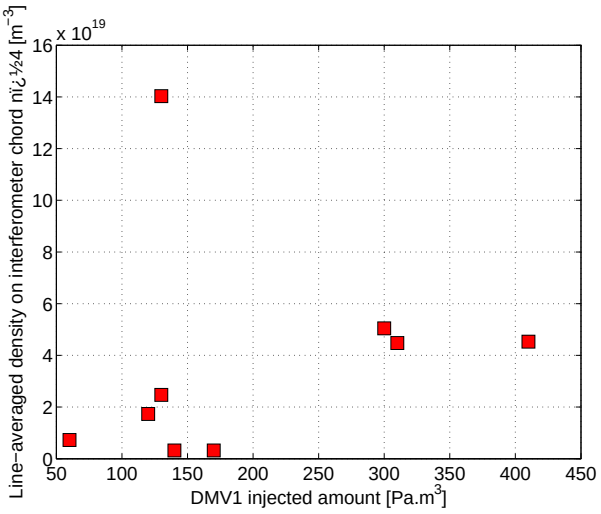

Figure 7. Density at the end of the runaway plateau seen by interferometer chord n4 as a function of the amount of argon injected by DMV1

- If the RE energy energy is such as $E_{K1} < E_{RE} < E_{K2}$, it will be accelerated asymptotically to E_{K2}.
- If the RE energy is higher than E_{K2}, it will be slowed down to E_{K2}.

In the present case, REs with energies more than 120 keV will be accelerated and REs with energies more than 21 MeV will be slowed down. Figure 9 shows the energy evolution in time for 4 different primary RE energies. One has to note that the actual duration of the RE beam in JET experiments is shorter than the time needed to reach the asymptotical $E_{K2} = 21$ MeV. However, the order of magnitude of this limit is in agreement with the measured RE energy spectrum (see section 3.3).

The minimum stopping power for the case presented here is $dEdX_{min}1.4$ MeV.cm^{2}g^{-1} which corresponds to a loss power per runaway electron of $\delta P_{min} = dEdX_{min}\beta c d_n = 345$ MeV.s^{-1} where $d_n = 8.2 \times 10^{-9}$ g.cm^{-3} is the argon density related to an argon density $n_{Ar0} = 1.24 \times 10^{20}$ m^{-3}. This corresponds to 22 MW transferred from the beam to the background plasma for a 1 MA RE beam case. This is enough to create the cold background plasma observed during the experiments. Following another approach, one can use the ionization cross section for argon σ_{Ar} as proposed in [41] to obtain the average ionization rate $\beta_e c \sigma_{Ar} = 2.54 \times 10^{-14}$ m^{-3}s^{-1}, leading to a argon ion density per second $n_{Ar+} = n_{RE} n_{Ar0} < \beta_e c \sigma_{Ar} > \approx 4 \times 10^{22}$ m^{-3}s^{-1} for a 1 MA RE beam. The amount of injected argon atoms could thus be theoretically ionized in less than 3 ms. This does not take into account multiple ionizations nor recombinations. Nonetheless this shows that a significant interaction between the runaway beam and the injected neutrals takes place. This plasma may play an important role in the runaway beam dynamics during mitigation attempts.

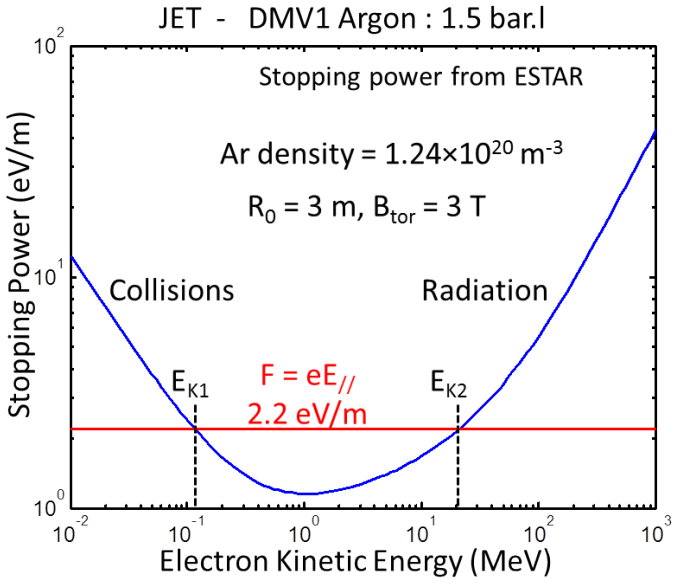

Figure 8. Stopping power for electrons in Argon gas in JPN87940. Below 1 MeV, the stopping power is dominated by collisions (Compton, Ionization). Above 1 MeV the slowing down is dominated by radiation (Bremsstrahlung). The electric driving force F = eE// gives a net acceleration between EK1 and EK2. Otherwise the drag force will overcome the driving force.

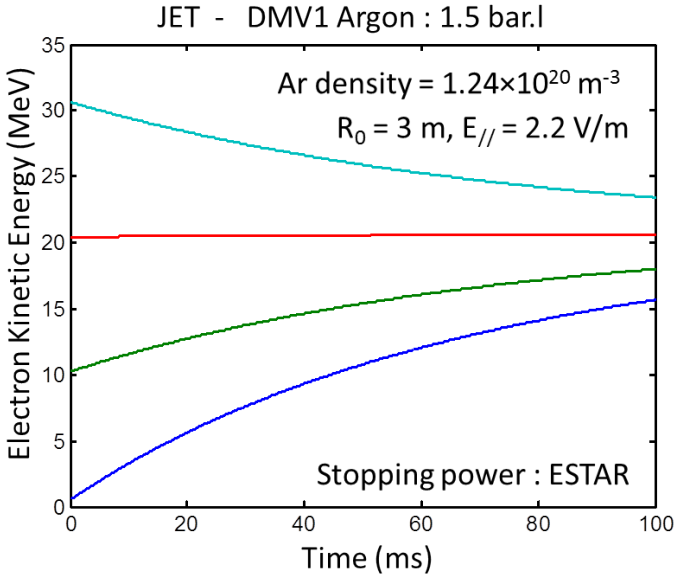

Figure 9. Kinetic energy evolution of runaway electrons taking into account the stopping power in Argon gas (from ESTAR) and the driving force generated by the toroidal electric field, for 4 initial electron energies.

4.2. Runaway beam early mitigation

Suppressing the runaway beam before it is fully developed is one of the options which is considered for future machines. This method was assessed using the following scheme at JET:

- DMV1 is fired with pure argon and relatively low pressure (from 130 Pa.m^3 to 170 Pa.m^3 injected), following the runaway beam scenario described in the previous section.
- DMV2 is fired with pure deuterium at moderate to high pressures (from 330 Pa.m^3 to 1900 Pa.m^3) at different times with respect to the DMV1 injection.

If DMV1 and DMV2 are fired at the same time, the overall mixture (neglecting propagation time effects) is roughly equivalent to a 90% D_2+10% Ar mix which is known not to produce runaways. As described before, firing DMV1 alone would lead to a 0.7-1.0 MA RE beam. The result of the DMV2 timing scan is shown on figure 10. The time reference used to compute the DMV2 injection time is the thermal quench of the disruption that would have happened if DMV1 was fired alone. As shown, the transition between complete runaway beam suppression (not even HXR traces) and the RE region is very sharp (1.7 ms timing difference for full pressure DMV2). The transition corresponds approximately to the onset of the thermal quench: firing DMV2 before the thermal quench completely suppresses runaway generation whereas firing DMV2 after the thermal quench has no effect on the runaway generation. The location of this transition was confirmed to be reproducible by repeating both cases (before and after TQ). This shows that suppressing primary runaways before the development of the full runaway beam through the avalanche is a viable solution using light gases such as deuterium.

A closer look to the transition between the complete runaway suppression situation and the fully-blown runaway beam is given on figure 11. It shows that the line integrated density before the thermal quench (measurements are not valid during the early current quench) and the electric field during the beginning of the current quench are similar for both pulses. This means that the plasma density during at the end of the thermal quench/beginning of the current quench (where unfortunately no measurements are available) is very different between the two cases presented here. The critical phase for early runaway suppression is thus the thermal quench. The DMV2 gas is mixed into the plasma most likely thanks to the large MHD activity during this phase of the disruption. Once the plasma is cold, the mixing efficiency drops: neutral gas which is not available at the thermal quench is probably not assimilated into the current quench plasma. The fact that HXR emissions start almost immediately after the plasma current spike also shows that the thermal quench is the critical phase for early runaway suppression. It is also to be noted that the plasma vertical motion is different in the two cases shown here: the runaway beam drifts upwards whereas the unmitigated disruptive plasma goes downwards. It is yet unclear if the difference in vertical motion is a cause or consequence

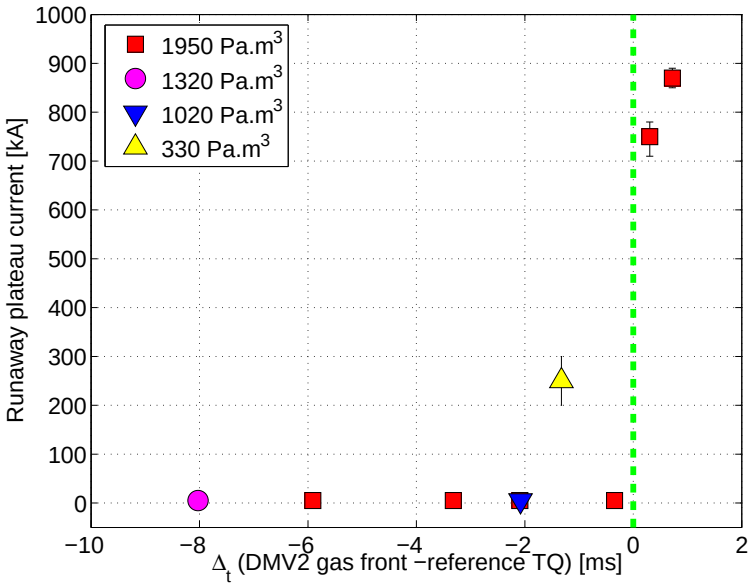

Figure 10. Runaway beam early mitigation. Runaway current as a function of DMV2 firing time with respect to the thermal quench of the DMV1-only disruption

of the runaway appearance, but stresses the importance of studying the vertical stability in the context of runaway beams.

A smoother transition was obtained by reducing the DMV2 deuterium pressure as shown on figure 10. Starting from the point where the runaway beam is suppressed by a high pressure DMV2 deuterium injection, the amount was reduced in two steps. In this case, the RE beam appears when the gas mixture assimilated during the thermal quench is no longer fit for runaway suppression (too high fraction of argon in the D2/Ar mixture).

4.3. Late current mitigation

Runaway mitigation before the thermal quench will not be necessarily feasible in all cases on ITER. In particular, injecting sufficient amounts of deuterium while keeping a quick enough current quench might be difficult, as deuterium alone tends to produce too slow, low-radiating current quenches [30]. Consequently, suppression of a fully-blown runaway beam must also be considered. Such experiments were carried out mainly using high-Z gases at JET (argon, krypton, xenon) as it is expected that the high pitch-angle scattering and higher stopping power associated with such gases will increase runaway losses. The following scenario is used:

- DMV1 is fired with pure argon (from 70 Pa.m^3 to 410 Pa.m^3 injected), following the runaway beam scenario described in the previous section.
- DMV2 is fired with different gases (D_2, Ar, Kr, Xe) at moderate to high pressures (from 330 Pa.m^3 to 4340 Pa.m^3) at different times during the runaway beam.

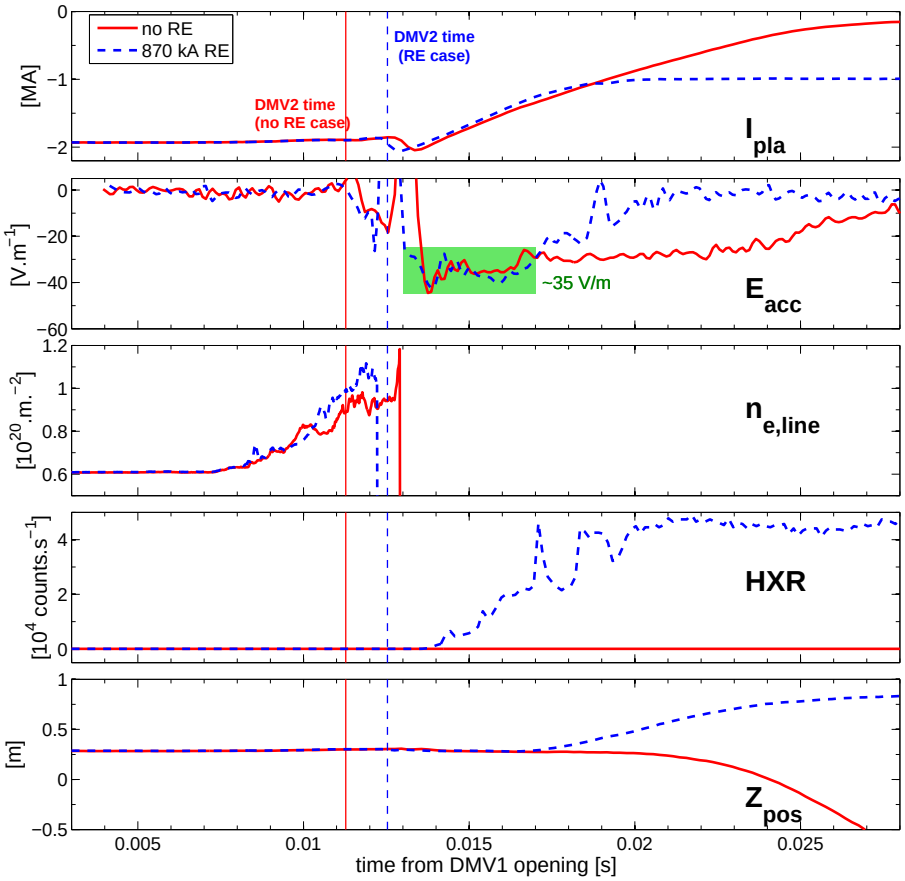

Figure 11. Runaway beam early mitigation - detail of the transition. (a) Plasma current (b) Accelerating electric field (c) line-integrated density (d) Hard X-ray total count rate (e) Current centroid vertical position

An example of such a mitigation attempt is shown on figure 12: DMV1 triggers the disruption with 120 Pa.m^3 argon and DMV2 is fired during the runaway beam with 2472 Pa.m^3 pure xenon. As shown on the figure, no significant effect on the RE beam parameters is observed. The plasma current decay is similar to the natural decay in an unmitigated RE beam as shown previously on figure 6. There is no change on the HXR/neutron rates nor on the current centroid movement following the DMV2 injection. Line integrated density measurements show a steady increase, but this increase also occurs in an unmitigated runaway beam as discussed in section 4.1. The effect of the DMV2 gas can however be seen on the soft X-ray cameras, showing a slight increase on chords viewing the center of the runaway beam as it drifts upwards. The fast visible camera also confirms some interaction between the RE beam and the DMV2 gas as the visible radiation increases quickly after the injection (see figure 12. This is only qualitative though, and the magnitude or the spectrum of such radiation cannot be inferred from unfiltered camera pictures.

Other attempts using different gases have been made and are summarized on figure 13(a). Although the longest runaway beam ever produced at JET-ILW is the

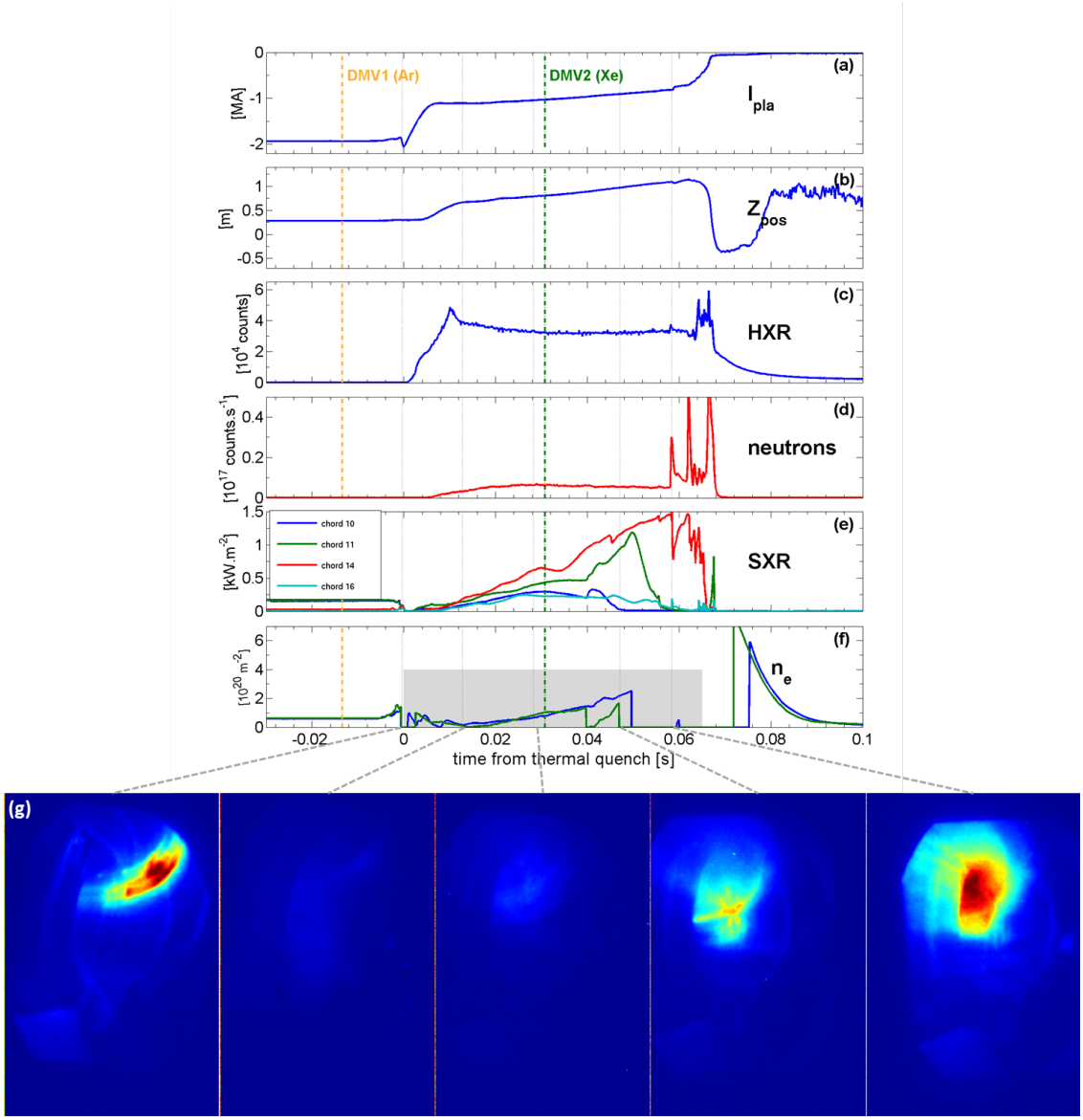

Figure 12. Runaway electron beam mitigation using 2472 Pa.m^3 Xenon. (a) Plasma current (b) plasma centroid vertical position (c) Hard X-ray total count rate (d) neutrons rate (e) Soft X-ray signals on chords pointed at the RE beam centroid along its upwards movement (f) Line integrated density - gray area represents relative signal variations only (reference is lost in the middle of the disruption) (g) fast camera pictures at different times

unmitigated one, this is likely to be a coincidence as there is no relation between the runaway current or the beam duration and the amount of gas injected. For instance, a 2120 Pa.m^3 xenon injection produced a longer RE beam than a 720 Pa.m^3 argon injection. Hard X-ray count rates reach the same order of magnitude in all cases as shown on figure 13(b). Figures 14(a) to (c) confirm the absence of any trend between the amount or the species injected by DMV2 in the beam and its main characteristics (slope, current, duration, Hard X-ray mean energy). Note that the DMV1 amount was

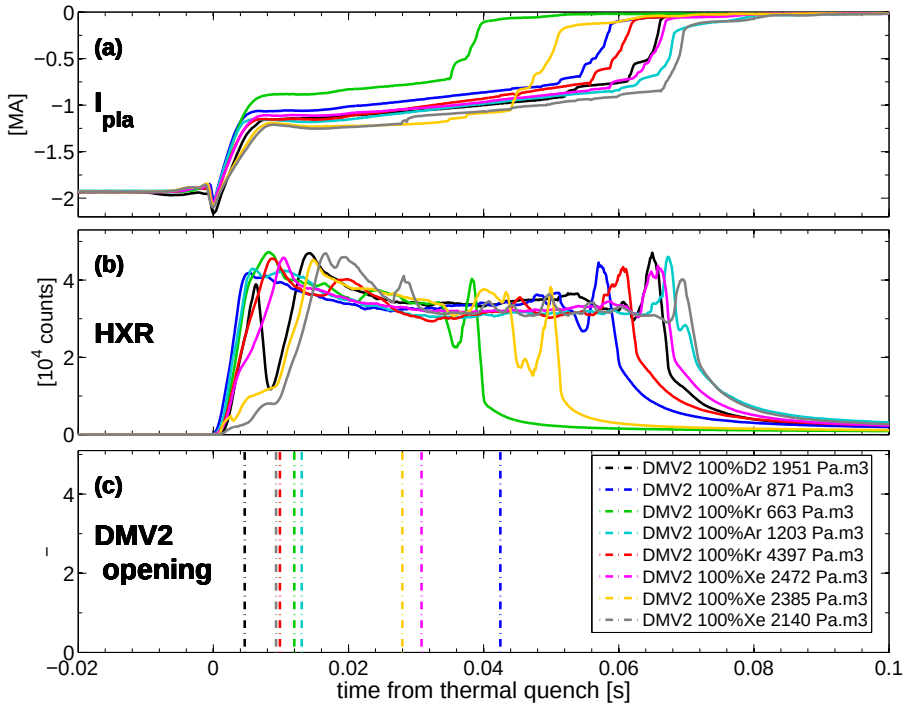

Figure 13. Summary of fully-blown RE beam mitigation attempts (a) Time traces of plasma current (b) Time traces of HXR count rates

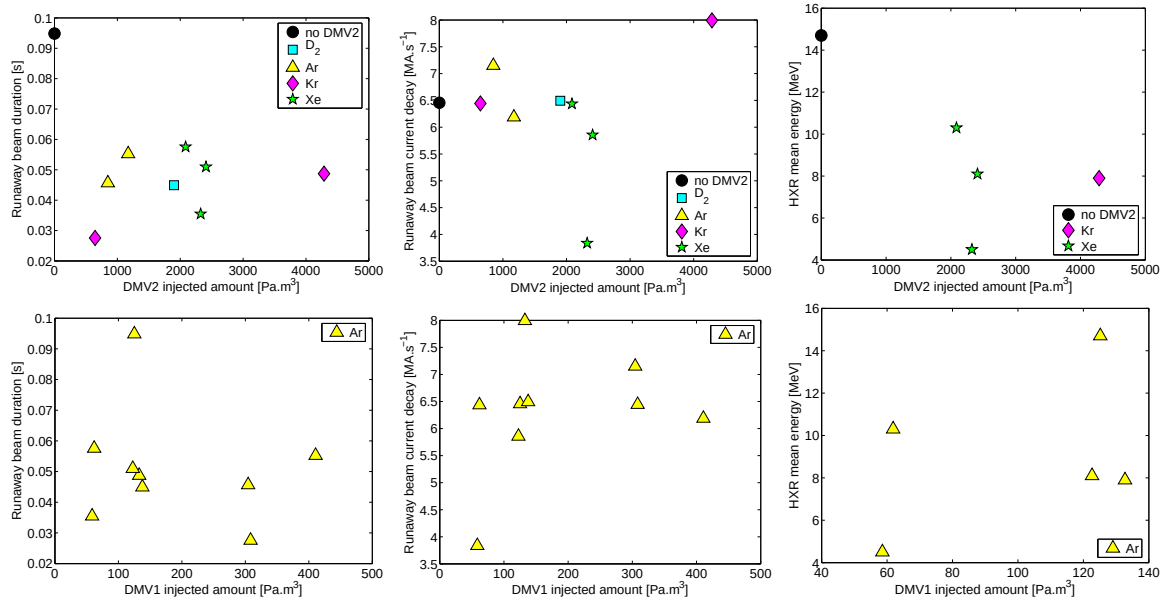

Figure 14. Runaway beam parameters as a function of DMV2 or DMV2 injection scenario (a) RE Beam duration as a function of DMV2 scenario (b) RE current mean decay rate as a function of DMV2 injection scenario (c) HXR mean energy as a function of the DMV2 scenario (d) RE beam duration as a function of the DMV1 injection scenario (d) RE current decay rate as a function of DMV1 injection scenario (f) HXR mean energy as a function of the DMV1 scenario

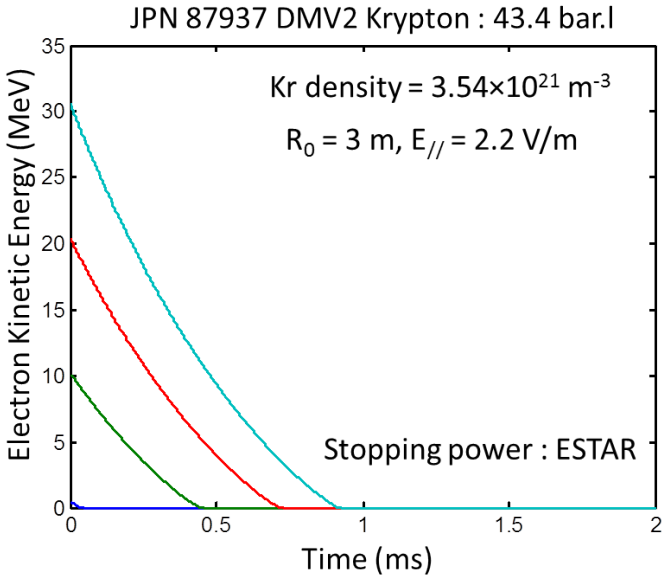

Figure 15. Kinetic energy evolution of runaway electrons taking into account the stopping power in Krypton massive gas injection on RE plateau flat-top and the driving force generated by the toroidal electric field, for 4 initial electron energies. The Ar impurity injected prior to disruption has been neglected.

also varied from 60 Pa.m^3 to 410 Pa.m^3 during experiments, based on the observation that the gas injected before the thermal quench had a large influence on the RE beam appearance as described in section 4.2. As shown on figure 14(d) to (f), there is no clear trend between the RE beam parameters and the DMV1 injection either.

The absence of effect of massive gas injection on an already accelerated RE beam contrasts with similar results obtained on smaller machines like DIII-D [14] and Tore Supra [8]. According to the ESTAR code, a complete thermalization of relativistic electrons should have taken place in less than 1 ms in the largest injection case (4340 Pa.m^3 krypton). Figure 15 shows the slowing down time for several RE energies. Although this estimate neglects the avalanche generation, the timespan available for runaway braking is two orders of magnitude higher than what is expected by the code, and it is still not enough. This clearly shows that injected neutrals do not penetrate into the RE beam region.

A number of hypotheses have been put forward to explain this lack of efficiency:

- The neutral/weakly ionized gas coming from DMV1 might impede the assimilation of the DMV2 gas into the RE beam region
- DMV is located on the midplane whereas the RE beam drifts upwards. Part of the gas plume might miss the region with highest RE current density.
- A pressure barrier due to the cold background plasma might impede the assimilation of the DMV2 gas into the RE beam region.
- A combination of those factors.

T[eV]	ξ_{in} [$10^{-}15\mathrm{m}^3\mathrm{s}^{-1}$] [44]	$\xi[10^{-15}\mathrm{m}^3\mathrm{s}^{-1}]$ [45]	L_{nf} [m]
2	1.2	0.018	0.30
5	1.7	2.9	0.02
10	2.2	18.3	0.005
15	2.6	36.1	0.003

Table 1. Thickness of the ionization layer L_{nf}, for several electron temperature in the layer

In order to address these questions, estimates of the thickness of the neutral diffusion and ionization layer were made. The simplified model described by Lehnert ([42, 43]) was used to come up with such estimates. It distinguishes a number of different edge plasma regimes, one of them being impermeable to neutrals. This regime is characterized by a ionization layer thinner than the neutral diffusion layer. The latter must also be thinner than the plasma radial dimension. This regime occurs when the ion and neutral density is high and when the ion temperature is high enough (more than 7-10 eV). Friction between ions and neutrals is then strong enough to create a large ion density in the edge of the neutral cloud, thus preventing neutrals from entering the plasma. The following paragraph will address the possibility of the background plasma being in such a regime.

Due to the strong charge exchange between ions and neutrals, ion and neutral temperatures are assumed to be equal to a mean diffusion layer temperature: $T_n \approx T_i \approx T_m$. Fast neutrals will thus determine the diffusion layer thickness. $T_m = 0.5eV$ as proposed in [42] is assumed for the purpose of this example calculation. The characteristic thickness of the diffusion layer is given by $L_d = 1/s_B = 1/(\mu_{in} \times \Gamma_0 \times \xi_{in}/(2kT_m))$ with $\mu_{in} = m_i m_n/(m_i + m_n)$ the reduced mass, m_i and m_n the ion and neutral mass, $\Gamma_0 = \Gamma_i = -n_i v_{ix} = \Gamma_n = n_n v_{nx}$ the ion and neutral fluxes and $\xi_{in} =< \sigma_{in} v_{in} >$ the average ion/neutral collision rate including charge exchange ($\sigma_{in} = \sigma_{in,el} + \sigma_{in,cx}$) where v_{in} is the relative ion-neutral velocity. In the JET case, with $n_i = 10^{20}\mathrm{m}^{-3}$ which is a reasonable estimate based on interferometry measurements (see section 4.1) and $\xi_{in} \approx 10^{-15}\mathrm{m}^3\mathrm{s}^{-1}$ [44], the boundary layer thickness is found to be close to 2 cm only.

According to [43], the ionization layer thickness is given by $L_{nf} = \left[2kT/\left(\mu_{in}\xi\left(\xi + \xi_{in}\right)\right)\right]^{1/2}/n_i$ where ξ is the ionization rate, n_i the average ion density and T the average temperature in the ionization layer. Charge exchange rate is taken from [44] and ionization rate as a function of temperature for argon is taken from [45]. Table 1 summarizes the ionization layer thickness L_{nf} for various ion temperatures.

In order to be in the impermeable plasma regime, the temperature at the edge of the background plasma must be larger than 10 eV (diffusion layer larger than the ionization layer). Estimates of the temperature of the background plasma are difficult to obtain. Nonetheless, analysis of spectral lines of argon during the runaway beam phase of similar experiments in JET-C tend to confirm the presence of Argon I, II and

III lines which require at least 27 eV temperature. This would confirm the impermeable plasma hypothesis, but contrasts with spectroscopy measurements made at DIII-D during runaway beams, which concluded $T_e \approx T_i \approx 1.6eV$ [14]. The major difference between JET and DIII-D is the magnitude of the runaway currents, 2 to 3 times higher at JET. This might explain a possibly higher background plasma temperature at JET.

It is to be noted that the runaway generation scenario used for the experiments (trigger the runaway beam using a high-Z injection and attempt mitigation using a second injection) is very similar to the ITER disruption mitigation scheme: mitigating heat loads with a first moderate to high-Z material injection then suppressing a possible runaway electron beam with another injection. If the background plasma created by the interaction between the gas from the first injection and the runaway beam at JET-ILW impedes the assimilation of the second gas puff into the RE region, it might have the same effect on ITER.

5. Runaway electron beam termination

5.1. Runaway electron beam final stages

As can be seen on figure 18, the beam termination is characterized by a fast drop in I_p and a succession of bursts of neutrons and magnetic fluctuations. In order to investigate possible reasons for this behavior, we analyze a database of 37 limiter pulses, both in carbon and ITER-like wall. Data is taken at the time of the first neutrons and magnetic fluctuations burst at the beginning of the termination phase of the beam. It should be mentioned that in many pulses, isolated bursts of neutrons and magnetic fluctuations are observed during the plateau phase, associated to small drops in I_p. However, we leave the analysis of these interesting events for future work.

Particular quantities of interest for our analysis are the minor radius a and the safety factor q_{edge} at the LCFS. Unfortunately, equilibrium reconstruction (for example with EFIT) is not available at the beam termination. Instead, we rely on the estimation of the toroidal current density centroid position ($R_{centroid}$, $Z_{centroid}$) based on magnetic measurements, which remains available throughout the pulse. The centroid position has been found to be rather consistent with the position of the geometric axis given by EFIT when it is available, although a vertical shift of approximately 10-15 cm exists. However, whether or not we take this vertical shift into account does not modify the general conclusions of our analysis. We assume the LCFS to have a circular cross-section at the time of the beam termination. Indeed, in discharges where EFIT reconstruction is available during the beginning of the runaway plateau, the ellipticity κ is found to decrease towards a value close to 1. The LCFS and its minor radius a are then found by looking for the point on the first wall that is closest to the centroid. We then estimate q_{edge} with the cylindrical formula: $q_{edge} = \frac{2\pi a^2 B_0 R_0}{(\mu_0 R^2_{centroid} I_p)}$ (where B_0 is the vacuum toroidal field at $R = R_0$). One should keep in mind that, given the uncertainties involved, we expect error bars of order 10 cm for a and 0.5-1 for q_{edge}.

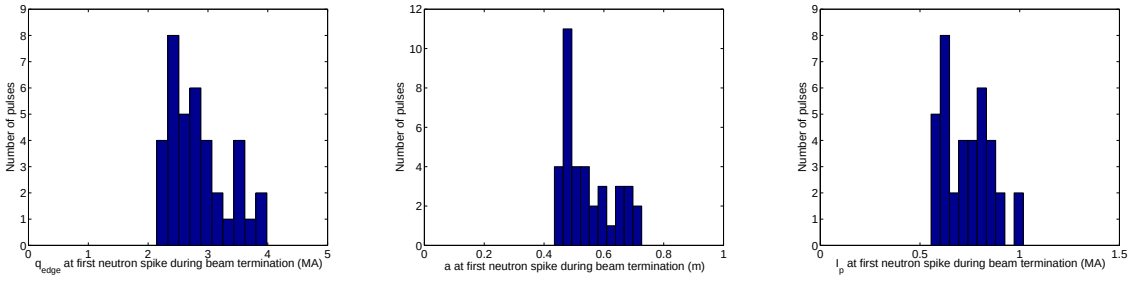

Figure 16. Analysis of the beam termination stage. Left: distribution of edge safety factor at termination. Middle: Distribution of minor radius. Right: Distribution of total current.

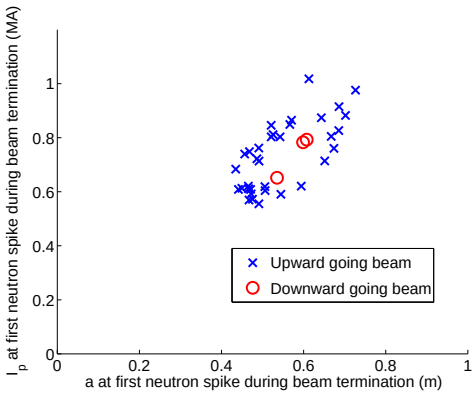

Figure 17. Correlation between plasma current and minor radius before the runaway beam final loss

Figure 16 shows a histogram of q_{edge} (left), a (middle) and I_p (right) at the beginning of the termination phase. It can be seen that q_{edge} lies between 2 and 4, with most pulses located between 2 and 3; a lies between 0.4 and 0.7 m with a peak at about 0.5 m; finally, I_p lies between 0.5 and 1.0 MA. We note that, given the width of the distributions of a and I_p and given the dependency of q_{edge} on these two quantities, one might expect, if these quantities were not correlated, a broader distribution of q_{edge}. In fact, as can be seen in Figure 17, a and I_p appear to be linearly correlated. Furthermore, one can see that downward going beams or upward going beams have similar Ip vs. a behavior. This observation of I_p vs. a, together with the fact that q_{edge} is close to 2-3 and with the presence of bursts of magnetic fluctuations, suggest that beam termination is related to MHD modes.

5.2. Runaway electron impact

The upward drift of the runaway beam leads it either to the upper dump plate or the upper parts of the inner wall limiters. Impacts of low runaway currents were already reported in [31] and showed that beryllium tile melting was unlikely below 150 kA runaways. A detailed analysis of the penetration of the electrons into the beryllium

showed that the energy was deposited over $2 \pm 1mm$ and that only part of the beam total energy was absorbed by a single tile. A significant part of the beam current simply goes through and hits the following tile along the toroidal direction. Impacts of such low currents were also found to be rather toroidally symmetrical.

Impacts of long runaway beams at higher currents show a different situation. An overview of a RE beam impact following a failed argon mitigation attempt is shown on figure 18. The beam maximum current starts at ≈ 1.0 MA and decays to 770 kA before the final loss. The upper part of the JET Inner Wall Guard Limiter is hit by the beam over a 10 cm^2 area per tile approximately. A maximum temperature of 1400C is measured by a fast infrared camera, and material ejection is clearly seen following the impact. Localized melting is thus certain and confirmed by in-vessel visual inspection of the tile. An important feature of this impact is that the interaction between the wall and the beam does not occur only during the final current drop. Although it is clear from the neutron/HXR spike that the main part of the interaction takes place during this phase, the tile heating starts before this final phase as shown by the temperature measurements (even taking into account the upper range of time stamp jitter of the device). The interaction between the tile and the beam may influence the way the final drop happens through induced currents into the material.

On the contrary to impacts on the upper dump plate, impacts on the inner limiters are very asymmetrical, as shown by in-vessel post-discharge inspections. The Inner Wall Guard Limiters at JET are made of 16 toroidally distributed poloidal beams which are supposed to be aligned within manufacturing tolerances. However, the tiles affected by the beam were not equally damaged. As figure 19 shows, only two of them show significant melting, two others only traces of very localized melting. Six tiles do not show any trace of damage. This pattern only partially overlaps the damage pattern which has been observed during limiter power handling experiments. The conditions in which melting was reached in both situations are of course different. But if limiter misalignment was solely responsible for the damage pattern, it would be similar in both experiments. The fact that the runaway impact often happens around a certain range of edge safety factors suggests that MHD instabilities could play a role in the impact pattern. The exact pattern relative to this presumed instability remains to be mapped to the observed damage once the JET vessel will be opened for a closer inspection of all the tiles for which no data is yet available.

6. Summary and discussion

Runaway electrons have been produced at JET in ITER-Like Wall configuration using massive injections of high-Z gases into divertor and limiter plasmas. The runaway existence domain was found to be similar to what it was at JET in Carbon Wall. This shows that the content of the post-MGI disruption plasma is dominated by the injected impurity and that the wall has only limited influence. Runaway electron generation in divertor configurations is found to be in agreement with Dreicer and avalanche

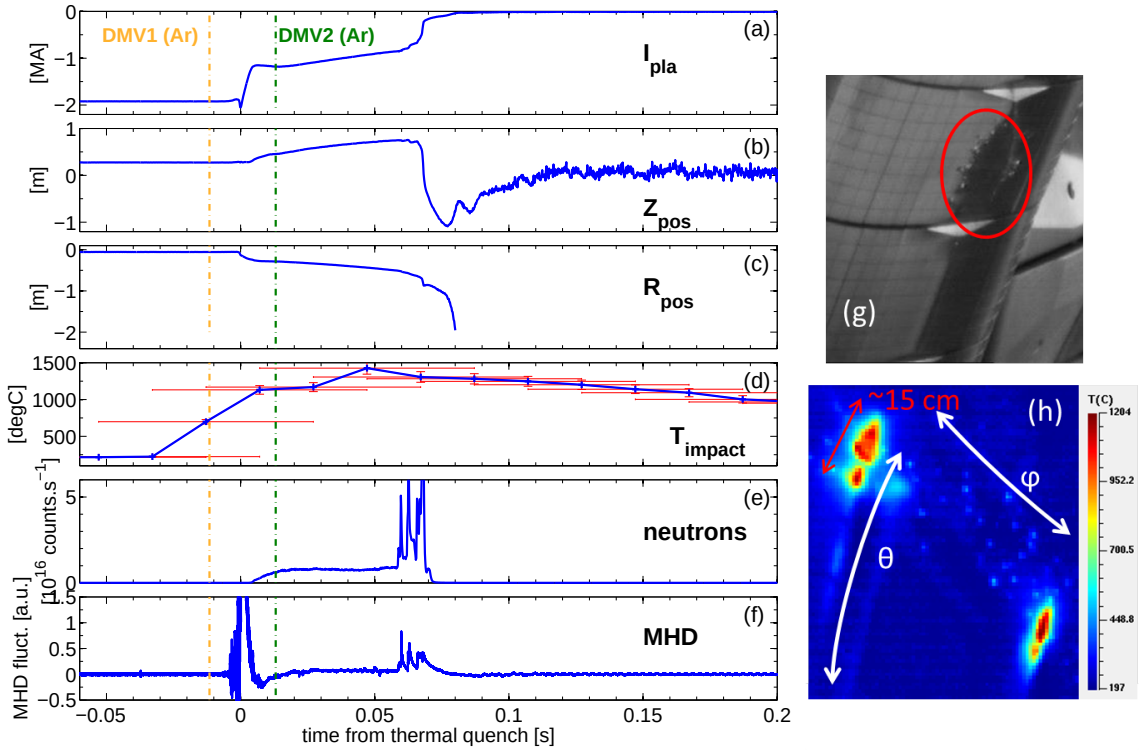

Figure 18. RE beam impact overview (a) Plasma current. (b) Plasma centroid vertical position (c) Plasma centroid radial position. (d) Neutron counts. (e) Surface temperature at impact. (f) MHD fluctuations (g) Visual inspection of damaged tile. (h) Infrared picture of the impact.

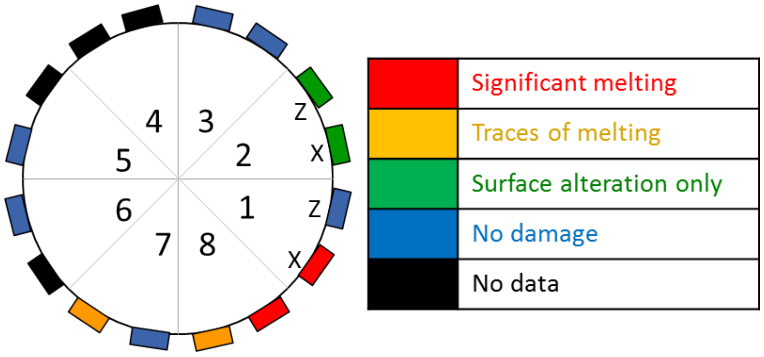

Figure 19. Tile damage on the JET Inner Wall Guard Limiter as observed by post-discharge in-vessel inspection (top view, octants numbers)

mechanisms and include the ratio between the accelerating electric field and the critical field for the avalanche mechanism and the toroidal magnetic field. A correlation with the magnetic turbulence is also observed. Limiter discharges do not follow the same trends, as they can generate up to 1 MA runaway beams for the same toroidal field, ratio of electric fields and magnetic turbulence as divertor pulses which do not show any signs of runaways. This together with the general trend that low elongation tokamaks generate more often runaways electrons points to a strong dependence of runaway existence on

the plasma shaping. Mechanisms involved in this behavior are not determined but may involve vertical stability or different ergodization dynamics of the plasma edge in limiter configurations. Energies up to 21 MeV have been observed during long runaway plateaux, in agreement with the usual range in large tokamaks. Runaway electron beams created by massive gas injection create a dense background plasma through collisions between the relativistic electrons and the injected neutrals. This plasma can reach a few $10^{19}\mathrm{m}^{-3}$ even far away from the RE beam and fills the major part of the vacuum vessel. Calculations of the power transferred from the RE beam to the background plasma as well as calculation of the ionization rate of the neutrals support this model of a cold dense background created by collisions and confined by the runaway current.

Runaway mitigation has been attempted and was found successful if deuterium neutrals are injected before the thermal quench. The gas assimilation drops after the large mixing occurring during MHD phase of the thermal quench and can no longer prevent runaway acceleration. Runaway mitigation after the beam has been accelerated has been proven unsuccessful at JET, with injections of 663 $\mathrm{Pa.m}^3$ to 4340 $\mathrm{Pa.m}^3$ of argon, krypton or xenon. None of the runaway parameters (current, duration, HXR production rate, total radiation, movement) shows any significant effect of the second injection. The interaction between the gas coming from the second injection and the runaway beam can only be confirmed by visible light from a fast camera and a moderate increase of soft X-ray signals. The absence of effect of the second injection is attributed to a very poor penetration of the gas into the runaway beam region. If the assimilation was complete, the runaway beam would have been stopped in a few milliseconds. This poor mixing is likely to be due to a screening effect by the cold background plasma which is in a neutral-impermeable regime. Impacts of runaway electrons on beryllium plasma-facing components led to localized melting with temperatures of 1400C for approximately 770 kA runaway beams. Large toroidal asymmetries are observed for high currents whereas lower current impacts on the top of the machine were more symmetrical. The origin of this asymmetry is unlikely to be only due to tile misalignments and may related to the instabilities leading to the runaway final loss on the wall.

These results confirm globally that runaway physics are similar with a metallic wall than with carbon wall, and that runaway electron suppression should be attempted before the beam is fully developed. Trying to suppress a fully-blown runaway beam which follows a massive gas injection intended at mitigating other effects of the disruption (electromagnetic loads, thermal loads) might be even more difficult than suppressing a natural runaway beam (i.e. without massive injection). More experiments and simulations are needed to understand if this feature can be overcome by other material injections scenarios. Other ways to control or suppress runaways by taking advantage of their generation or loss dependencies should also be studied.

Acknowledgements

This work has been carried out within the framework of the EUROfusion Consortium and has received funding from the European Unions Horizon 2020 research and innovation programme under grant agreement number 633053. The views and opinions expressed herein do not necessarily reflect those of the European Commission or the ITER Organization.

[1] V.S. Vlasenkov, V.M. Leonov, V.G. Merezhkin, and V.S. Mukhovatov. The runaway electron discharge regime in the tokamak-6 device. *Nuclear Fusion*, 13(4):509, 1973.

[2] R.D. Gill. Generation and loss of runaway electrons following disruptions in jet. *Nuclear Fusion*, 33(11):1613, 1993.

[3] V.V. Plyusnin, V. Riccardo, R. Jaspers, B. Alper, V.G. Kiptily, J. Mlynar, S. Popovichev, E. de La Luna, F. Andersson, and JET EFDA contributors. Study of runaway electron generation during major disruptions in jet. *Nuclear Fusion*, 46(2):277, 2006.

[4] M. Lehnen, S.S. Abdullaev, G. Arnoux, S.A. Bozhenkov, M.W. Jakubowski, R. Jaspers, V.V. Plyusnin, V. Riccardo, and U. Samm. Runaway generation during disruptions in {JET} and {TEXTOR}. *Journal of Nuclear Materials*, 390391(0):740 – 746, 2009. Proceedings of the 18th International Conference on Plasma-Surface Interactions in Controlled Fusion Device Proceedings of the 18th International Conference on Plasma-Surface Interactions in Controlled Fusion Device.

[5] G. Arnoux et al. Heat load measurements on the jet first wall during disruptions. *Journal of Nuclear Materials*, 415(1, Supplement):S817 – S820, 2011. Proceedings of the 19th International Conference on Plasma-Surface Interactions in Controlled Fusion.

[6] R. Yoshino, Y. Neyatani, N. Hosogane, S.W. Wolfe, M. Matsukawa, and H. Ninomiya. The softening of current quenches in jt-60u. *Nuclear Fusion*, 33(11):1599, 1993.

[7] R. Yoshino, S. Tokuda, and Y. Kawano. Generation and termination of runaway electrons at major disruptions in jt-60u. *Nuclear Fusion*, 39(2):151, 1999.

[8] F. Saint-Laurent, C. Reux, J. Bucalossi, A. Loarte, S. Bremond, C. Gil, P. Moreau, and J.L. Segui. Control of runaway electron beams on tore supra. *Proceedings of the 36th EPS Conf. on Plasma Physics vol 33E P-4.205*, 2009.

[9] F. Saint-Laurent, C. Reux, S. Bremond, D. Douai, C. Gil, and P. Moreau. Control of runaway electron beam heat loads on tore supra. *Proceedings of the 38th EPS Conf. on Plasma Physics vol 33E O3.118*, 2011.

[10] K.H. Finken, J.G. Watkins, D. Rusbldt, W.J. Corbett, K.H. Dippel, D.M. Goebel, and R.A. Moyer. Observation of infrared synchrotron radiation from tokamak runaway electrons in textor. *Nuclear Fusion*, 30(5):859, 1990.

[11] M. Lehnen, S. Bozhenkov, S. Abdullaev, and M. Jakubowski. Suppression of runaway electrons by resonant magnetic perturbations in textor disruptions. *Phys. Rev. Lett.*, 100:255003, Jun 2008.

[12] E.M. Hollmann, P.B. Parks, D.A. Humphreys, N.H. Brooks, N. Commaux, N. Eidietis, T.E. Evans, R. Isler, A.N. James, T.C. Jernigan, J. Munoz, E.J. Strait, C. Tsui, J. Wesley, and J.H. Yu. Effect of applied toroidal electric field on the growth/decay of plateau-phase runaway electron currents in diii-d. *Nuclear Fusion*, 51(10):103026, 2011.

[13] N. W. Eidietis, N. Commaux, E. M. Hollmann, D. A. Humphreys, T. C. Jernigan, R. A. Moyer, E. J. Strait, M. A. VanZeeland, J. C. Wesley, and J. H. Yu. Control of post-disruption runaway electron beams in diii-da). *Physics of Plasmas (1994-present)*, 19(5):–, 2012.

[14] E.M. Hollmann, M.E. Austin, J.A. Boedo, N.H. Brooks, N. Commaux, N.W. Eidietis, D.A. Humphreys, V.A. Izzo, A.N. James, T.C. Jernigan, A. Loarte, J. Martin-Solis, R.A. Moyer, J.M. Muoz-Burgos, P.B. Parks, D.L. Rudakov, E.J. Strait, C. Tsui, M.A. Van Zeeland, J.C.

Wesley, and J.H. Yu. Control and dissipation of runaway electron beams created during rapid shutdown experiments in diii-d. *Nuclear Fusion*, 53(8):083004, 2013.

[15] B. Esposito, J. R. Martn-Sols, F. M. Poli, J. A. Mier, R. Snchez, and L. Panaccione. Dynamics of high energy runaway electrons in the frascati tokamak upgrade. *Physics of Plasmas (1994-present)*, 10(6):2350–2360, 2003.

[16] E.D. Fredrickson, M.G. Bell, G. Taylor, and S.S. Medley. Control of disruption-generated runaway plasmas in tftr. *Nuclear Fusion*, 55(1):013006, 2015.

[17] M.N. Rosenbluth and S.V. Putvinski. Theory for avalanche of runaway electrons in tokamaks. *Nuclear Fusion*, 37(10):1355, 1997.

[18] T.C. Hender, J.C Wesley, J. Bialek, A. Bondeson, A.H. Boozer, R.J. Buttery, A. Garofalo, T.P Goodman, R.S. Granetz, Y. Gribov, O. Gruber, M. Gryaznevich, G. Giruzzi, S. Gnter, N. Hayashi, P. Helander, C.C. Hegna, D.F. Howell, D.A. Humphreys, G.T.A. Huysmans, A.W. Hyatt, A. Isayama, S.C. Jardin, Y. Kawano, A. Kellman, C. Kessel, H.R. Koslowski, R.J. La Haye, E. Lazzaro, Y.Q. Liu, V. Lukash, J. Manickam, S. Medvedev, V. Mertens, S.V. Mirnov, Y. Nakamura, G. Navratil, M. Okabayashi, T. Ozeki, R. Paccagnella, G. Pautasso, F. Porcelli, V.D. Pustovitov, V. Riccardo, M. Sato, O. Sauter, M.J. Schaffer, M. Shimada, P. Sonato, E.J. Strait, M. Sugihara, M. Takechi, A.D. Turnbull, E. Westerhof, D.G. Whyte, R. Yoshino, H. Zohm, Disruption the ITPA MHD, and Magnetic Control Topical Group. Chapter 3: Mhd stability, operational limits and disruptions. *Nuclear Fusion*, 47(6):S128, 2007.

[19] L. Zeng, H. Koslowski, Y. Liang, A. Lvovskiy, M. Lehnen, D. Nicolai, J. Pearson, M. Rack, H. Jaegers, K. Finken, K. Wongrach, Y. Xu, and the TEXTOR team. Experimental observation of a magnetic-turbulence threshold for runaway-electron generation in the textor tokamak. *Phys. Rev. Lett.*, 110:235003, Jun 2013.

[20] T. Flp, G. Pokol, P. Helander, and M. Lisak. Destabilization of magnetosonic-whistler waves by a relativistic runaway beam. *Physics of Plasmas (1994-present)*, 13(6):–, 2006.

[21] T. Flp, H. M. Smith, and G. Pokol. Magnetic field threshold for runaway generation in tokamak disruptions. *Physics of Plasmas (1994-present)*, 16(2):–, 2009.

[22] M. Lehnen, A. Alonso, G. Arnoux, N. Baumgarten, S.A. Bozhenkov, S. Brezinsek, M. Brix, T. Eich, S.N. Gerasimov, A. Huber, S. Jachmich, U. Kruezi, P.D. Morgan, V.V. Plyusnin, C. Reux, V. Riccardo, G. Sergienko, M.F. Stamp, and JET EFDA contributors. Disruption mitigation by massive gas injection in jet. *Nuclear Fusion*, 51(12):123010, 2011.

[23] E.M. Hollmann, T.C. Jernigan, M. Groth, D.G. Whyte, D.S. Gray, M.E. Austin, B.D. Bray, D.P. Brennan, N.H. Brooks, T.E. Evans, D.A. Humphreys, C.J. Lasnier, R.A. Moyer, A.G. McLean, P.B. Parks, V. Rozhansky, D.L. Rudakov, E.J. Strait, and W.P. West. Measurements of impurity and heat dynamics during noble gas jet-initiated fast plasma shutdown for disruption mitigation in diii-d. *Nuclear Fusion*, 45(9):1046, 2005.

[24] N. Commaux, L.R. Baylor, S.K. Combs, N.W. Eidietis, T.E. Evans, C.R. Foust, E.M. Hollmann, D.A. Humphreys, V.A. Izzo, A.N. James, T.C. Jernigan, S.J. Meitner, P.B. Parks, J.C. Wesley, and J.H. Yu. Novel rapid shutdown strategies for runaway electron suppression in diii-d. *Nuclear Fusion*, 51(10):103001, 2011.

[25] C. Reux, J. Bucalossi, F. Saint-Laurent, C. Gil, P. Moreau, and P. Maget. Experimental study of disruption mitigation using massive injection of noble gases on tore supra. *Nuclear Fusion*, 50(9):095006, 2010.

[26] F. Saint-Laurent, G. Martin, T. Alarcon, A. Le Luyer, P. Pastor, S. Putvinski, B. Vincent, J. Bucalossi, S. Bremond, Ph. Moreau, E. Nardon, and C. Reux. Fire, a novel concept of massive gas injection for disruption mitigation in iter: Validation on tore supra. *Fusion Engineering and Design*, 89(12):3022 – 3038, 2014.

[27] R.D. Gill, B. Alper, M. de Baar, T.C. Hender, M.F. Johnson, V. Riccardo, and contributors to the EFDA-JET Workprogramme. Behaviour of disruption generated runaways in jet. *Nuclear Fusion*, 42(8):1039, 2002.

[28] U. Kruezi, P.D. Morgan, M. Lehnen, S. Bozhenkov, S. Jachmich, M.F. Stamp, I. Coffey,

S. Brezinsek, P.C. de Vries, G. Sergienko, G.F. Matthews, K.H. Finken, A. Savtchkov, and JET EFDA contributors. Massive gas injection experiments at jet - performance and characterisation of the disruption mitigation valve. In *Proceedings of the 36th EPS Conference on plasma Physics, Sofia, Bulgaria*, 2009.

[29] U. Kruezi, H.R. Koslowski, S. Jachmich, M. Lehnen, S. Brezinsek, G.F. Matthews, and JET EFDA contributors. A new disruption mitigation system for deuteriium-tritium operation at jet. In *Proceedings of the 28th Symposium on Fusion Technology SOFT, San Sebastian, Spain*, 2014.

[30] M. Lehnen, G. Arnoux, S. Brezinsek, J. Flanagan, S.N. Gerasimov, N. Hartmann, T.C. Hender, A. Huber, S. Jachmich, V. Kiptily, U. Kruezi, G.F. Matthews, J. Morris, V.V. Plyusnin, C. Reux, V. Riccardo, B. Sieglin, P.C. de Vries, and JET EFDA Contributors. Impact and mitigation of disruptions with the iter-like wall in jet. *Nuclear Fusion*, 53(9):093007, 2013.

[31] C. Reux, V. Plyusnin, B. Alper, D. Alves, B. Bazylev, E. Belonohy, S. Brezinsek, J. Decker, S. Devaux, P. de Vries, A. Fil, S. Gerasimov, I. Lupelli, S. Jachmich, E.M. Khilkevitch, V. Kiptily, R. Koslowski, U. Kruezi, M. Lehnen, A. Manzanares, J. Mlyn, E. Nardon, E. Nilsson, V. Riccardo, F. Saint-Laurent, A.E. Shevelev, and C. Sozzi. Runaway beam studies during disruptions at jet-ilw. *Journal of Nuclear Materials*, (0):–, 2014.

[32] H. Dreicer. Electron and ion runaway in a fully ionized gas. i. *Phys. Rev.*, 115:238–249, Jul 1959.

[33] H. Dreicer. Electron and ion runaway in a fully ionized gas. ii. *Phys. Rev.*, 117:329–342, Jan 1960.

[34] J.W. Connor and R.J. Hastie. Relativistic limitations on runaway electrons. *Nuclear Fusion*, 15(3):415, 1975.

[35] F. Saint-Laurent, C. Reux, J. Bucalossi, A. Loarte, S. Bremond, C. Gil, P. Maget, P. Moreau, and J.L. Segui. Disruption and runaways electron mitigation studies on tore supra. In *Proceedings of the 23rd IAEA Fusion Energy Conference, Daejon, REp. of Korea*, 2010.

[36] A.E. Shevelev et al. Reconstruction of distribution functions of fast ions and runaway electrons in fusion plasmas using gamma-ray spectrometry with applications to iter. *Nuclear Fusion*, 53(12):123004, 2013.

[37] S. Brezinsek, T. Loarer, V. Philipps, H.G. Esser, S. Grnhagen, R. Smith, R. Felton, J. Banks, P. Belo, A. Boboc, J. Bucalossi, M. Clever, J.W. Coenen, I. Coffey, S. Devaux, D. Douai, M. Freisinger, D. Frigione, M. Groth, A. Huber, J. Hobirk, S. Jachmich, S. Knipe, K. Krieger, U. Kruezi, S. Marsen, G.F. Matthews, A.G. Meigs, F. Nave, I. Nunes, R. Neu, J. Roth, M.F. Stamp, S. Vartanian, U. Samm, and JET EFDA contributors. Fuel retention studies with the iter-like wall in jet. *Nuclear Fusion*, 53(8):083023, 2013.

[38] M.J. Berger, J.S. Coursey, M.A. Zucker, and J. Chang. Estar, pstar, and astar: computer programs for calculating stopping-power and range tables for electrons, protons, and helium ions. version 1.2.3, [online]., 2005.

[39] International Commission on Radiation Units and Measurements. Stopping powers for electrons and positrons, 1984.

[40] M. Bakhtiari, G. Kramer, M. Takechi, H. Tamai, Y. Miura, Y. Kusama, and Y. Kamada. Role of bremsstrahlung radiation in limiting the energy of runaway electrons in tokamaks. *Phys. Rev. Lett.*, 94:215003, Jun 2005.

[41] Foster Rieke and William Prepejchal. Ionization cross sections of gaseous atoms and molecules for high-energy electrons and positrons. *Phys. Rev. A*, 6:1507–1519, Oct 1972.

[42] B. Lehnert. Screening of a high-density plasma from neutral gas penetration. *Nuclear Fusion*, 8(3):173, 1968.

[43] B. Lehnert. Plasma-neutral gas boundary layers. *Nuclear Instruments and Methods*, 129(1):31 – 37, 1975.

[44] E. Salzborn. Charge exchange cross sections. *Nuclear Science, IEEE Transactions on*, 23(2):947–958, April 1976.

[45] G.S. VORONOV. A practical fit formula for ionization rate coefficients of atoms and ions by electron impact (z=1-28). *Atomic Data and Nuclear Data Tables*, 65(1):1 – 35, 1997.